

Thermal Decomposition of Spherically Granulated Malachite: Physico-Geometrical Constraints and Overall Kinetics

Yuta Aoki, Yui Yamamoto, and Nobuyoshi Koga*

Department of Science Education, Division of Educational Sciences, Graduate School of Humanity and Social Sciences, Hiroshima University, 1-1-1 Kagamiyama, Higashi-Hiroshima 739-8524, Japan

Contents

S1. Setup of TG–DTA Instruments	s2
S2. Sample Characterization	s3
Figure S1. XRD pattern of the sample.....	s3
Figure S2. FT-IR spectrum of the sample.....	s3
Table S1. Assignments of IR absorption peaks ³⁹⁻⁴⁴	s3
Figure S3. SEM images of the sample particles (before sieving).....	s3
Figure S4. Particle-size distribution of the sample particles (before sieving).....	s3
S3. Thermal Behavior.....	s4
Figure S5. Changes in XRD pattern during stepwise isothermal heating of granular malachite: (a) XRD patterns at different temperatures, (b) at 773 K, and (c) changes in the intensity of the diffraction peaks attributed to CuO with increasing the temperature and crystallite size of CuO.	s4
Figure S6. Changes in XRD pattern during isothermal heating of granular malachite at 513 K: (a) XRD patterns at different duration times, (b) after heating for 285 min, and (c) changes in the intensity of the diffraction peaks attributed to CuO with the duration time at 513 K and the crystallite size of CuO.	s4
Figure S7. Changes in the surface texture of the granular particles heated to different temperatures at a β of 10 K min^{-1} in a stream of dry N_2 gas (flow rate = 300 $\text{cm}^3 \text{min}^{-1}$): (a) $T = 462 \text{ K}$ ($\alpha = 0.00$), (b) $T = 507 \text{ K}$ ($\alpha = 0.02$), (c) $T = 535 \text{ K}$ ($\alpha = 0.11$), (d) $T = 556 \text{ K}$ ($\alpha = 0.35$), (e) $T = 564 \text{ K}$ ($\alpha = 0.57$), and (f) $T = 596 \text{ K}$ ($\alpha = 0.98$).	s5
Figure S8. Changes in the surface texture of the granular particles heated at a constant temperature ($T = 498 \text{ K}$) for different duration times in a stream of dry N_2 gas (flow rate = 300 $\text{cm}^3 \text{min}^{-1}$): (a) 8 min ($\alpha = 0.02$), (b) 53 min ($\alpha = 0.14$), (c) 311 min ($\alpha = 0.63$), and (d) 589 min ($\alpha = 0.99$).	s5
Figure S9. TG–DTG curves for the thermal decomposition of granular malachite with different particle size fractions, recorded using approximately 5.0 mg of sample in a stream of dry N_2 gas and heated at a β of 2 K min^{-1}	s5
S4. Mathematical Deconvolution Analysis.....	s6
Figure S10. Typical results of MDA for the thermal decomposition of the granular malachite under (a) isothermal and (b) linear nonisothermal conditions.	s6
Table S2. Kinetic parameters determined by MDA and subsequent isoconversional kinetic analysis for the mathematically separated kinetic curves	s6
Figure S11. Mathematically separated kinetic curves for each reaction step under isothermal conditions: (a) first and (b) second reaction steps.....	s7
Figure S12. Mathematically separated kinetic curves for each reaction step under linear nonisothermal conditions: (a) first and (b) second reaction steps.....	s7
Figure S13. Results of the conventional isoconversional kinetic calculation applied to the mathematically separated kinetic curves for each reaction step: (a) Friedman plots for the first reaction step, (b) Friedman plots for the second reaction step, and (c) $E_{a,i}$ values at different α values.....	s7
Figure S14. Experimental master plots for the first and second reaction steps calculated from the mathematically separated kinetic curves.....	s8
S5. Kinetic Deconvolution Analysis	s8
Table S3. Kinetic parameters optimized via KDA for the thermal decomposition of granular malachite under linear nonisothermal conditions.....	s8

* Corresponding author. E-mail: nkoga@hiroshima-u.ac.jp

S1. Setup of TG–DTA Instruments

Three TG–DTA instruments used in this study were all configured using horizontal thermobalances. Preliminary to the measurements, all instruments were calibrated with regard to temperature and mass-change value. The temperature calibration was made with reference to the onset temperature of the melting endotherms of Ga, In, Sn, Pb, Zn, Al, and Ag (purity > 99.99%, Nilaco) recorded by heating at a β of 5 K min^{-1} in flowing dry N_2 or He. The mass-change value was initially calibrated by addition/removal of a standard weight of a 10 mg to/from the sample holder of the balance system. Thereafter, the mass-loss values of each reaction step of thermal dehydration/decomposition of $\text{CaC}_2\text{O}_4 \cdot \text{H}_2\text{O}$ (> 99.9985%, Alfa Aesar) were confirmed by recording TG curves at a β of 5 K min^{-1} under the respective atmospheric conditions used for the sample measurements.

The sample mass of 5.0 mg was selected as the largest value, but not form layer in the platinum sample pan of 5 mm in diameter and 2.5 mm in depth. Appropriate flow rate of dry N_2 gas for the horizontal thermobalance was selected by comparing the TG–DTA curves of the present sample recorded at a β of 5 K min^{-1} in flowing dry N_2 at different rates in a range of $50\text{--}500 \text{ cm}^3 \text{ min}^{-1}$. Because no changes were observed for the TG–DTA curves recorded at a flow rate larger than $200 \text{ cm}^3 \text{ min}^{-1}$, a flow rate of $300 \text{ cm}^3 \text{ min}^{-1}$ was selected for the measurements in flowing dry N_2 gas. For the TG/DTA–MS measurements in flowing He, a lower flow rate of $200 \text{ cm}^3 \text{ min}^{-1}$ was selected to increase the concentration of evolved gas for MS measurements.

S2. Sample Characterization

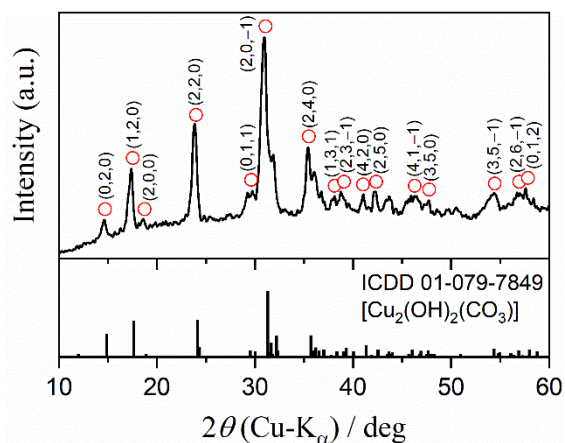


Figure S1. XRD pattern of the sample.

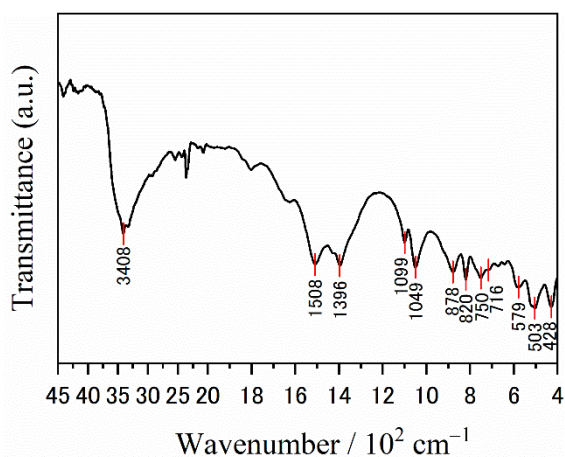


Figure S2. FT-IR spectrum of the sample.

Table S1. Assignments of IR absorption peaks³⁹⁻⁴⁴

Peak position /cm ⁻¹	Vibration mode
3408	ν O-H
1508, 1396	ν_3 , CO ₃ ²⁻
1099	ν_1 , CO ₃ ²⁻
1049, 878	O-H out of plane bending
820	ν_2 , CO ₃ ²⁻
750, 716	ν_4 , CO ₃ ²⁻
579, 503	ν Cu-O
428	ν Cu-X

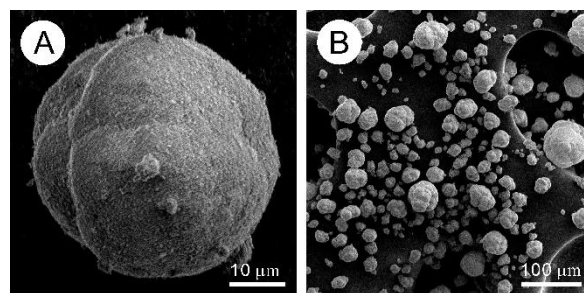


Figure S3. SEM images of the sample particles (before sieving).

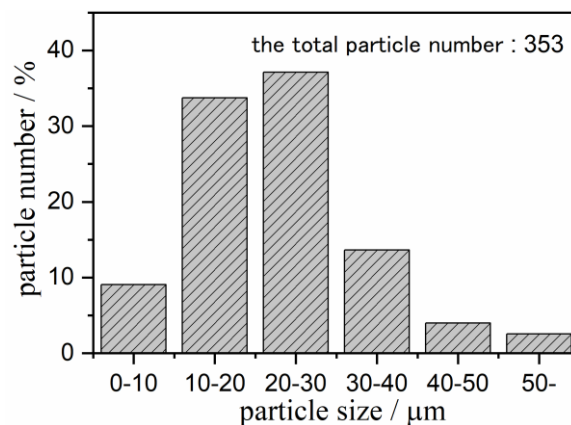


Figure S4. Particle-size distribution of the sample particles (before sieving).

S3. Thermal Behavior

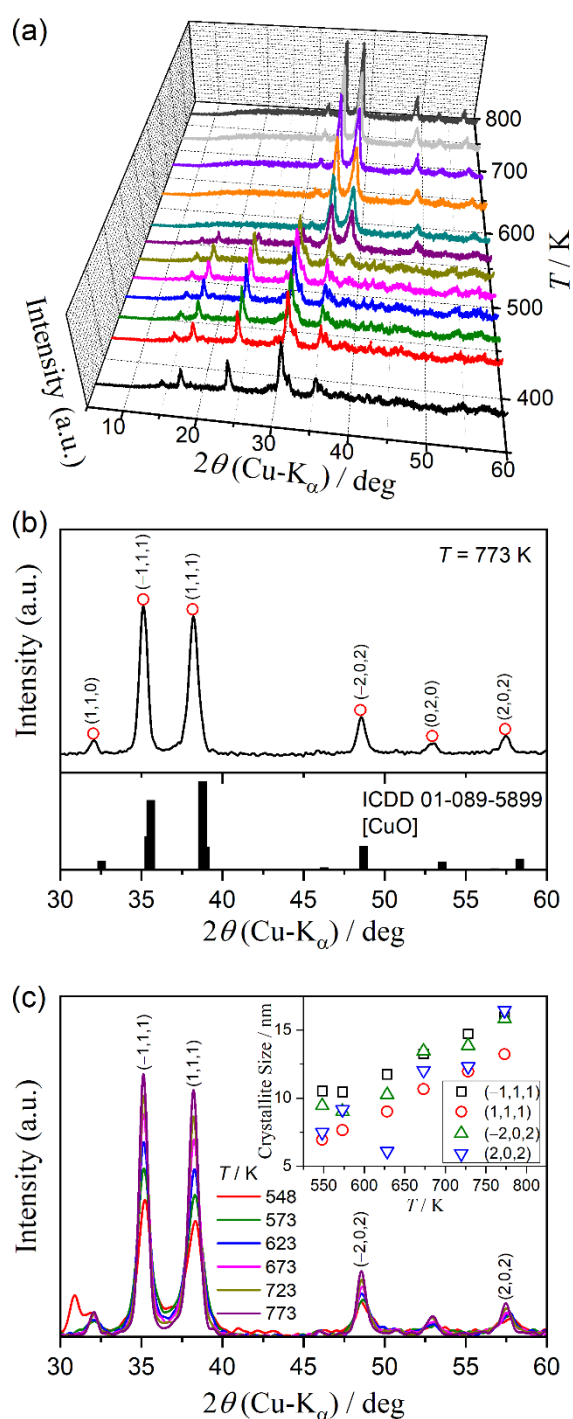


Figure S5. Changes in XRD pattern during stepwise isothermal heating of granular malachite: (a) XRD patterns at different temperatures, (b) at 773 K, and (c) changes in the intensity of the diffraction peaks attributed to CuO with increasing the temperature and crystallite size of CuO.

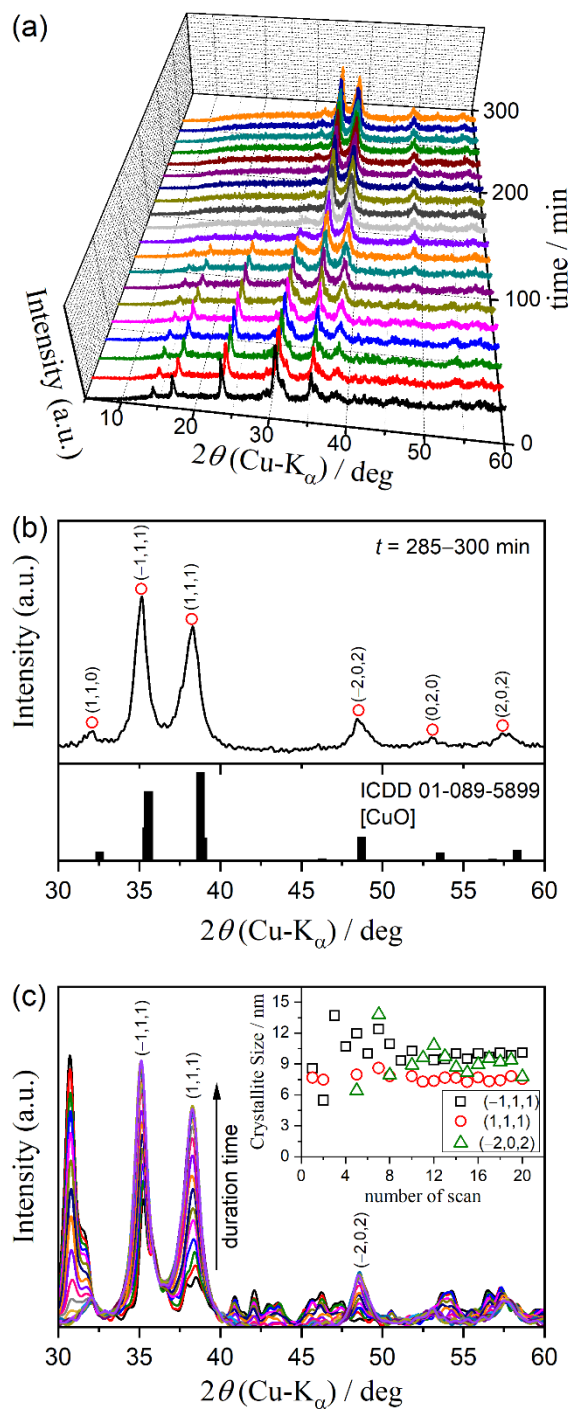


Figure S6. Changes in XRD pattern during isothermal heating of granular malachite at 513 K: (a) XRD patterns at different duration times, (b) after heating for 285 min, and (c) changes in the intensity of the diffraction peaks attributed to CuO with the duration time at 513 K and the crystallite size of CuO.

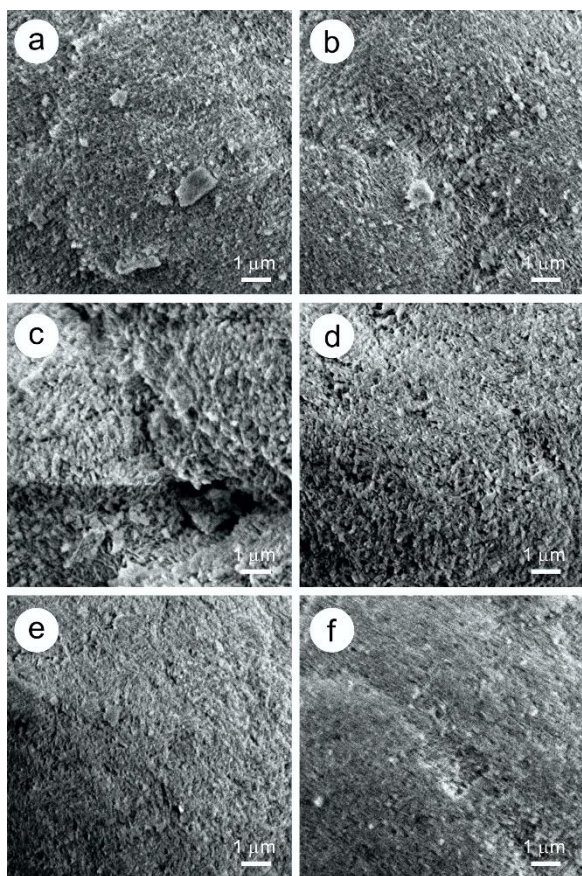


Figure S7. Changes in the surface texture of the granular particles heated to different temperatures at a β of 10 K min^{-1} in a stream of dry N_2 gas (flow rate = $300 \text{ cm}^3 \text{ min}^{-1}$): (a) $T = 462 \text{ K}$ ($\alpha = 0.00$), (b) $T = 507 \text{ K}$ ($\alpha = 0.02$), (c) $T = 535 \text{ K}$ ($\alpha = 0.11$), (d) $T = 556 \text{ K}$ ($\alpha = 0.35$), (e) $T = 564 \text{ K}$ ($\alpha = 0.57$), and (f) $T = 596 \text{ K}$ ($\alpha = 0.98$).

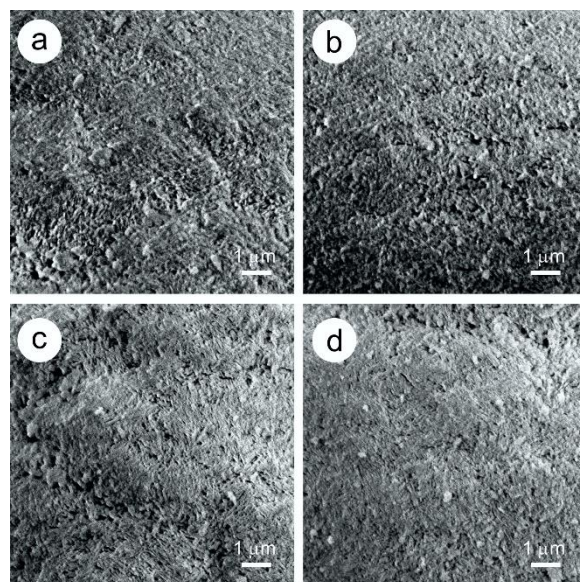


Figure S8. Changes in the surface texture of the granular particles heated at a constant temperature ($T = 498 \text{ K}$) for different duration times in a stream of dry N_2 gas (flow rate = $300 \text{ cm}^3 \text{ min}^{-1}$): (a) 8 min ($\alpha = 0.02$), (b) 53 min ($\alpha = 0.14$), (c) 311 min ($\alpha = 0.63$), and (d) 589 min ($\alpha = 0.99$).

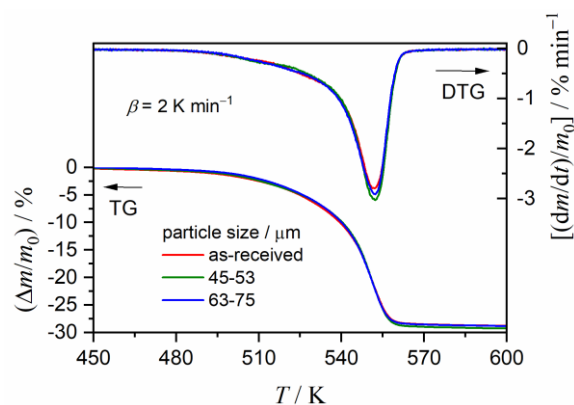


Figure S9. TG–DTG curves for the thermal decomposition of granular malachite with different particle size fractions, recorded using approximately 5.0 mg of sample in a stream of dry N_2 gas and heated at a β of 2 K min^{-1} .

S4. Mathematical Deconvolution Analysis

The DTG curves for the thermal decomposition of the granular malachite recorded under isothermal and linear nonisothermal conditions were subjected to MDA, for which the Weibull function was selected as an appropriate function among different types of the statistical distribution functions.

■ Weibull function:

$$F(t) = a_0 \left(\frac{a_3 - 1}{a_3} \right)^{\frac{1-a_3}{a_3}} \left\{ \frac{t - a_1}{a_2} + \left(\frac{a_3 - 1}{a_3} \right)^{\frac{1}{a_3}} \right\}^{a_3 - 1} \exp \left[- \left\{ \frac{t - a_1}{a_2} + \left(\frac{a_3 - 1}{a_3} \right)^{\frac{1}{a_3}} \right\}^{a_3} + \frac{a_3 - 1}{a_3} \right] \quad (\text{S1})$$

where a_0 – a_3 are the amplitude, center, width, and shape, respectively.

Figure S10 shows typical results of MDA applied to the thermal decomposition of the granular malachite under isothermal and linear nonisothermal conditions. The initial c_i values estimated from the peak areas of partially overlapping peaks are listed in Table S2. A series of kinetic curves for the individual reaction steps were obtained from the separated DTG curves by MDA, as shown in Figures S11 and S12 for the reactions under isothermal and nonisothermal conditions, respectively.

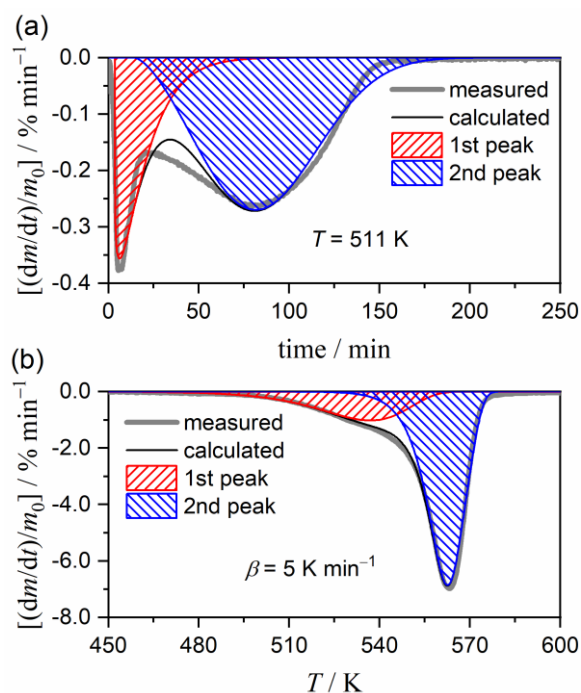


Figure S10. Typical results of MDA for the thermal decomposition of the granular malachite under (a) isothermal and (b) linear nonisothermal conditions.

Table S2. Kinetic parameters determined by MDA and subsequent isoconversional kinetic analysis for the mathematically separated kinetic curves

i	c_i	$E_{a,i} / \text{kJ mol}^{-1}$	A_i / s^{-1}	$f_i(\alpha_i) = \alpha_i^{m_i} (1 - \alpha_i)^{n_i} [-\ln(1 - \alpha_i)]^{p_i}$		
				m_i	n_i	p_i
1	0.25 ± 0.02	147.6 ± 10.1	$(1.15 \pm 0.03) \times 10^{12}$	-0.68 ± 0.19	1.17 ± 0.07	0.67 ± 0.18
2	0.75 ± 0.02	147.6 ± 1.9	$(6.05 \pm 0.02) \times 10^{11}$	-0.13 ± 0.02	1.04 ± 0.01	0.75 ± 0.02

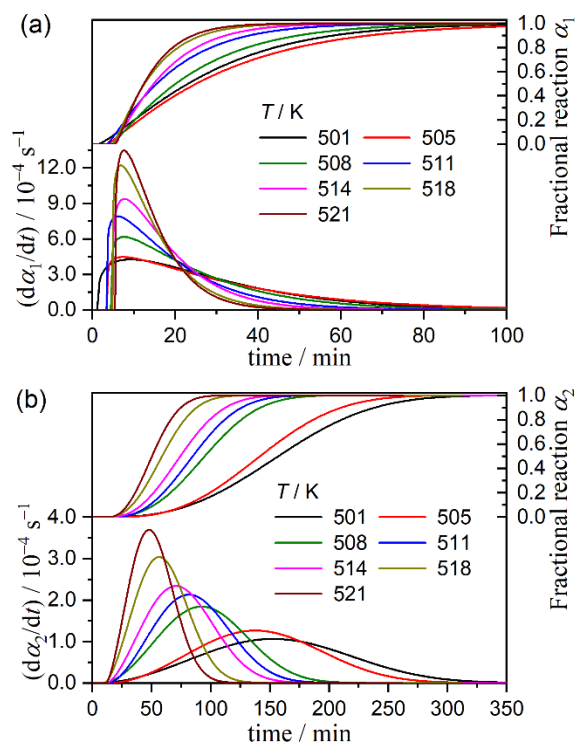


Figure S11. Mathematically separated kinetic curves for each reaction step under isothermal conditions: (a) first and (b) second reaction steps.

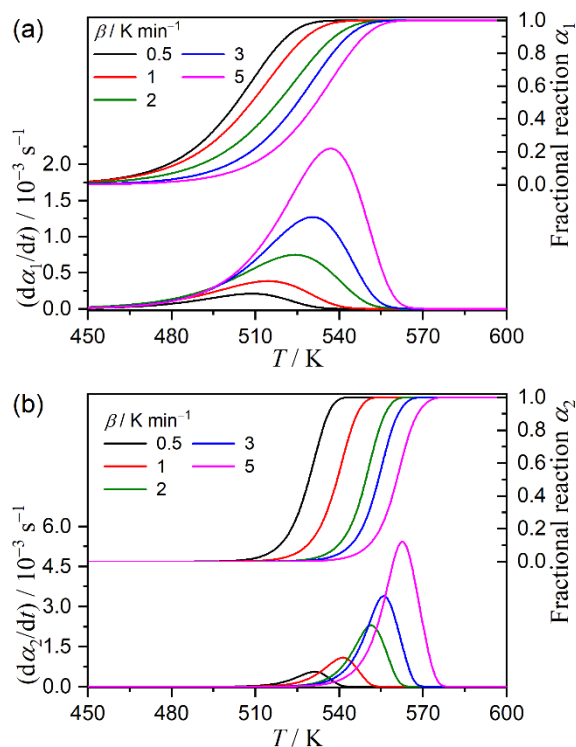


Figure S12. Mathematically separated kinetic curves for each reaction step under linear nonisothermal conditions: (a) first and (b) second reaction steps.

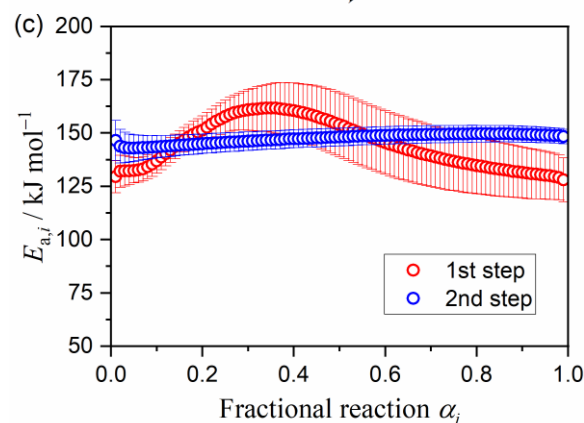
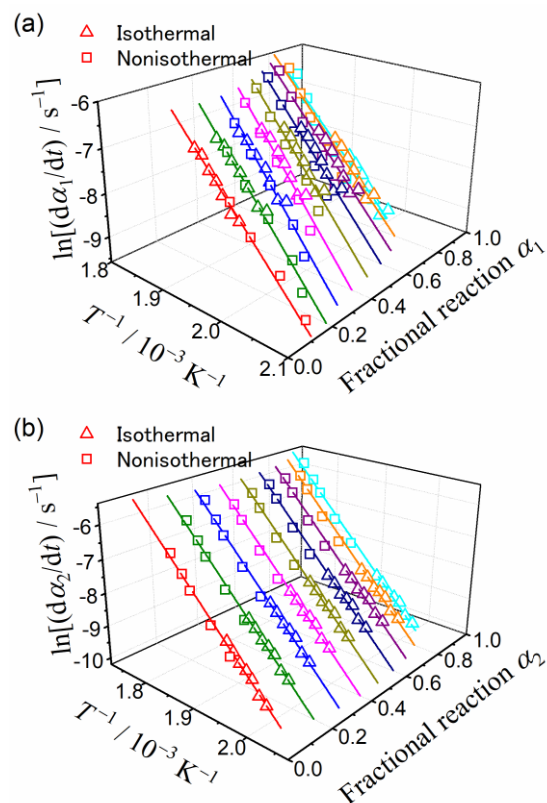


Figure S13. Results of the conventional isoconversional kinetic calculation applied to the mathematically separated kinetic curves for each reaction step: (a) Friedman plots for the first reaction step, (b) Friedman plots for the second reaction step, and (c) $E_{a,i}$ values at different α_i values.

The mathematically generated kinetic curves for each reaction step under isothermal and linear nonisothermal conditions were analyzed using the conventional isoconversional method (eq. (3)). Figure S13 summarizes the results of the isoconversional kinetic calculation. For both reaction steps, statistically significant linear correlations were observed for the Friedman plots at different α_i values (Figure S13(a) and

(b)). A detectable change in the slope of the Friedman plots as the reaction advanced was observed for the first reaction step, but not for the second reaction step. Therefore, the $E_{a,i}$ values changed with the progress of the reaction for the first reaction step and remained constant for the second reaction step (Figure S13(c)). However, the average E_a values for the first and second reaction steps in an α_i range of 0.1–0.9 were practically identical, as listed in Table S2.

Figure S14 shows the experimental master plots for each reaction step calculated according to eq. (7) using the average $E_{a,i}$ values. A linear deceleration of the reaction rate with the progress of the reaction is characteristic of the first reaction step. Meanwhile, the second reaction step exhibits the maximum rate midway through the reaction. The experimental master plots were fitted using $SB(m, n, p)$ to obtain the A_i

values and the kinetic exponents in the SB model to be used as the initial values for KDA. The results of the mathematical fitting of the experimental master plots are also listed in Table S2.

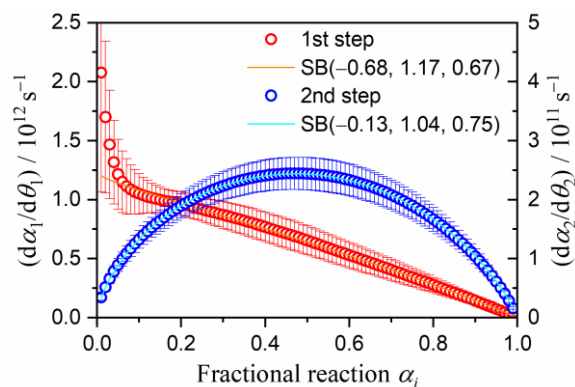


Figure S14. Experimental master plots for the first and second reaction steps calculated from the mathematically separated kinetic curves.

S5. Kinetic Deconvolution Analysis

Table S3. Kinetic parameters optimized via KDA for the thermal decomposition of granular malachite under linear nonisothermal conditions

$\beta / \text{K min}^{-1}$	i	c_i	$E_{a,i} / \text{kJ mol}^{-1}$	A_i / s^{-1}	$f_i(\alpha_i) = \alpha_i^{m_i}(1 - \alpha_i)^{n_i}[-\ln(1 - \alpha_i)]^{p_i}$			$R^{2, a}$
					m_i	n_i	p_i	
0.5	1	0.26	148.8	1.15×10^{12}	-0.68	1.17	0.67	0.9999
	2	0.74	148.6	6.04×10^{11}	-0.13	1.05	0.74	
1	1	0.27	148.6	1.15×10^{12}	-0.68	1.15	0.67	0.9999
	2	0.73	148.5	6.04×10^{11}	-0.13	1.00	0.75	
2	1	0.36	151.0	1.14×10^{12}	-0.83	1.06	0.53	0.9999
	2	0.64	147.4	5.88×10^{11}	-0.13	1.01	0.82	
3	1	0.32	149.1	1.15×10^{12}	-0.69	1.05	0.67	0.9999
	2	0.68	146.8	5.98×10^{11}	-0.13	1.04	0.82	
5	1	0.38	150.7	1.14×10^{12}	-0.80	0.86	0.59	0.9999
	2	0.62	145.6	5.69×10^{11}	-0.13	1.11	0.87	

^aDetermination coefficient of the nonlinear least-squares analysis of KDA.